Fatigue Crack Growth and Fracture Toughness Behavior of an Al-Li-Cu Alloy

K. V. JATA and E. A. STARKE, Jr.

Slip behavior, fracture toughness, and fatigue thresholds of a high purity Al-Li-Cu alloy with Zr as a dispersoid forming element have been studied as a function of aging time. The fracture toughness variation with aging time has been related to the changes in slip planarity, *i.e.*, slip band spacing and width. Although the current alloy exhibits planar slip for all aging conditions examined, the crack initiation toughness, K_{1c}, compares favorably with those of 2XXX and 7XXX aluminum alloys. Near threshold fatigue crack growth results in air and vacuum suggest that irregularities in the crack profile and the fracture surfaces and slip reversibility are some of the major contributing factors to the crack growth resistance of this alloy.

I. INTRODUCTION

AIRCRAFT designers are constantly striving to achieve minimum weight in order to cut fuel consumption and improve overall performance. Reducing the density of structural materials has been shown to be the most efficient solution to this problem.[1] Since aluminum alloys make up between seventy and eighty percent of the current aircraft weight, recent alloy development programs have focused on reducing the density of these materials.[2] Lithium additions to aluminum provide the greatest reduction in density of any alloying element and offer the additional advantage of increasing the elastic modulus. However, Al-Li-X alloys often exhibit low ductility and fracture toughness.

Various modifications in alloy chemistry and fabricating techniques have been used in an attempt to improve the ductility while maintaining a high strength. Copper, Mg, and Zr solute additions have been shown to have beneficial effects.[3] Magnesium and Cu improve the strength of Al-Li alloys through solid solution and precipitate strengthening, and can minimize the formation of precipitate free zones (PFZ) near grain boundaries. Zirconium, which forms the cubic Al_3Zr coherent dispersoid, stabilizes the subgrain structure and suppresses recrystallization.

The goals of most Al-Li-X alloy development programs include improvements in density and modulus with equivalent or improved damage tolerance and corrosion properties compared with currently used materials, *e.g.*, 7075 and 2024.[4] Although there have been numerous reports on the relationship among composition, microstructure, and monotonic properties of Al-Li-X alloys,[5,6] there have been few studies on the cyclic properties and fracture toughness of these materials. This paper describes the fatigue crack propagation and fracture toughness of a new alloy based on the Al-Li-Cu system which is somewhat related to the Al-Li-Cu alloy 2020 that was commercially available in the 1960's.

II. EXPERIMENTAL PROCEDURES

The actual chemical composition of the Al-Li-Cu alloy used for the present investigations is shown in Table I. It is similar in composition to the Al-Li-Cu alloy, M2, recently studied by Feng *et al.*,[7] except for slightly lower Cu and Cd and slightly higher Li contents. In addition to the above, low levels of Fe and Si were maintained to minimize the amount of constituent phases. Zirconium was added as the dispersoid forming element.

The material was obtained from Reynolds Metals Company in the form of 27.7 mm thick plates. The original cast ingots were homogenized in an argon atmosphere as follows: (i) heated at 523 K/hour to 673 K, held 48 hours, (ii) heated at 298 K/hour to 763 K, held 18 hours, (iii) heated at 298 K/hour to 788 K held for 30 minutes and fan cooled. The ingots were scalped on the surface to 69.8 mm thick and then cleaned. The hot rolling was performed in three steps, preheated to 733 K, held for one hour, hot rolled from 69.8 mm to 57.1 mm, reheated to 733 K, hot rolled to 44.5 mm, reheated to 671 K, and hot rolled to a final thickness to 27.7 mm.

The alloy was solutionized in a salt bath at 78 K for 30 minutes, quenched in ice water, stretched 2 pct, and aged in an oil bath at 433 K for different periods of time (Table II). Fracture toughness was measured on 11 mm thick compact tension samples in the L-T orientation, and a conditional K_{1c} value for fracture toughness was obtained from the load-crack opening displacement plots by choosing the 5 pct secant offset line. Of all the samples tested, only the two underaged samples did not meet the ASTM thickness criterion $b \geq 2.5\ (K_{1c}/\sigma_{ys})^2$. A thickness of 54 mm would have been required for the underaged samples for a valid K_{1c} test.

Crack propagation tests were conducted on compact tension specimens in laboratory air (R.H. ~ 45 pct) and a vacuum of 10^{-5} torr at 295 K using an R ratio of 0.1 and a frequency of 30 Hz. The crack propagated in the long transverse direction on a plane normal to the rolling direction. Crack growth was monitored with a traveling microscope and load *vs* crack opening displacement curves were generated by the elastic compliance techniques. Near threshold crack growth rates were obtained by the load-shedding scheme. At every load level the crack was allowed to propa-

Table I. Actual Chemical Composition in Weight Percent

Cu	Li	Cd	Zr	Fe	Si	Al
3.6	1.68	0.16	0.16	0.01	0.02	bal.

K. V. JATA, Research Assistant Professor, Department of Materials Science, and E. A. STARKE, Jr., Earnest Oglesby Professor of Materials Science and Dean, School of Engineering and Applied Science, are with The University of Virginia, Thornton Hall, Charlottesville, VA 22901.

Manuscript submitted April 11, 1985.

Table II. Mechanical Properties

Microstructure	Aging Time	σ_{ys} (MPa)	σ_{uts} (MPa)	Pct Elongation*	n	${}^{+}\varepsilon_f^T$	K_{1c}
UA-1	8 hours	300	431	20	0.13	0.3568	44
UA-2	12 hours	350	452	18	0.098	0.315	40
PA	17 hours	520	534	8	0.055	0.145	32.2
OA-1	19 hours	500	526	8.6	0.062	—	30
OA-2	22 hours	484	500	6.6	0.056	—	27
OA-3	26 hours	472	496	4.0	0.062	—	30

*as measured on 19 mm gage length.

${}^{+}\varepsilon_f^T = \ln\left(\frac{A_0}{A_f}\right)$; A_0 is the original and A_f is the final cross sectional area.

gate the distance equal to at least three times the cyclic plastic zone size, and then the load was decreased by less than 3 pct.

The microstructures were examined by optical, scanning, and transmission electron microscopy. Thin foils for transmission work were obtained with a dual jet Tenupol apparatus by using 50 pct nitric acid-methanol mixture at 253 K and a potential difference of 15 volts. Fracture surfaces were examined with a scanning electron microscope.

III. RESULTS AND DISCUSSION

A. *Microstructure and Tensile Properties*

Optical metallography revealed a predominately unrecrystallized grain structure. However, some recrystallization occurred during solution treatment as shown in the micrograph of the L-S section, Figure 1(a). A high degree of recrystallization has been shown to be undesirable in Al-Li-X alloys since secondary crack paths are invariably associated with recrystallized grains.[8] Thus from a ductility point of view, it is advantageous to select a low solutionization temperature in order to suppress recrystallization.[8] However, if the temperature is too low, some strength is lost due to incomplete solutionizing prior to aging. In the present work a solution treatment temperature of 788 K was found to be an optimum temperature to achieve the desired strength level, while minimizing the degree of recrystallization. No coarse precipitate, which would be associated with an incomplete solution heat treatment, was observed (Figure 1(a)).

A detailed TEM examination was performed to study the microstructure of the alloy. Bright-field images revealed the subgrains in the unrecrystallized structure to be approximately 5 microns in diameter (Figure 1(b)). Precipitate characterization was performed using an exact [100] zone to detect Al_3Li and Al_2Cu precipitates, and an exact [110] zone to detect Al_2CuLi precipitates.[9,10,11] The Al_3Li (δ') could not be imaged as individual precipitates in any aging condition using the Al_3Li-Al_3Zr superlattice spot shown in Figure 2(a). However, the "donut" contrast of the spherical precipitates shown in Figure 2(b) may indicate a ternary Al-Zr-Li phase.[12] Since it was impossible to isolate the Al_3Li-Al_3Zr superlattice spots from the streaking associated with the Θ' (Al_2Cu) phase, Θ' is also observed in Figure 2(b). The Θ' precipitates appeared as plates in two orthogonal directions and as a plate with a line of no-contrast as the third variant, Figure 2(b), consistent with previous observations.[13]

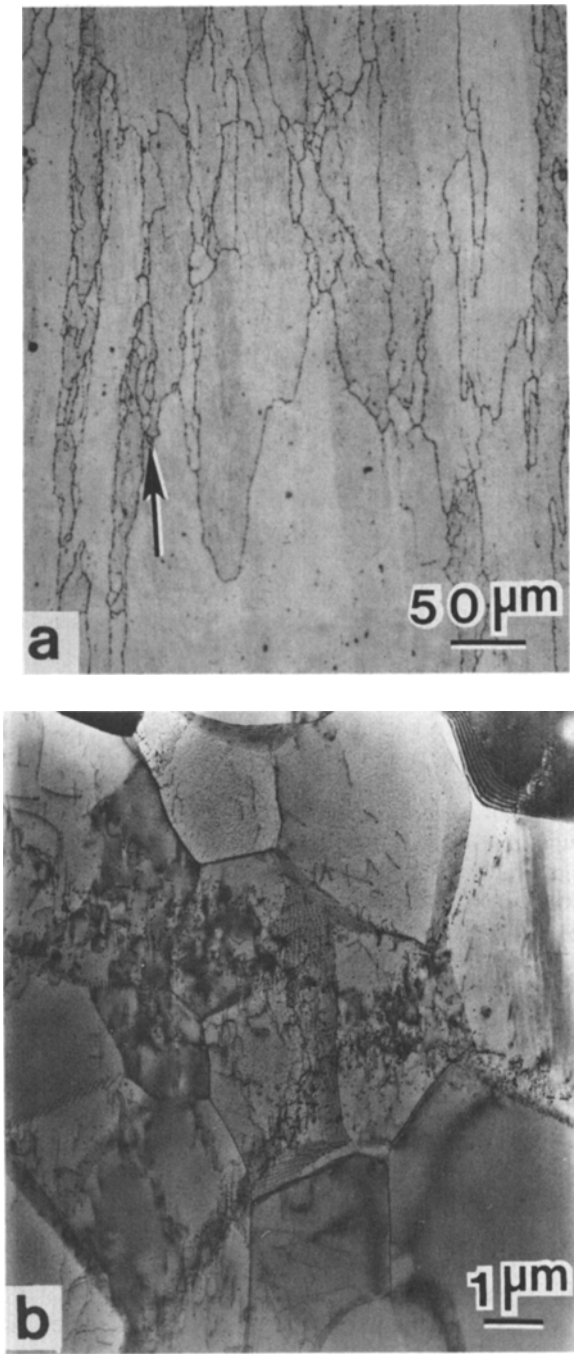

Fig. 1 — (*a*) Optical micrograph of the L-S section illustrating the large unrecrystallized grains and small recrystallized grains (shown by arrow) formed during the solution heat treatment, and (*b*) TEM of the subgrain structure in the {112} foil plane.

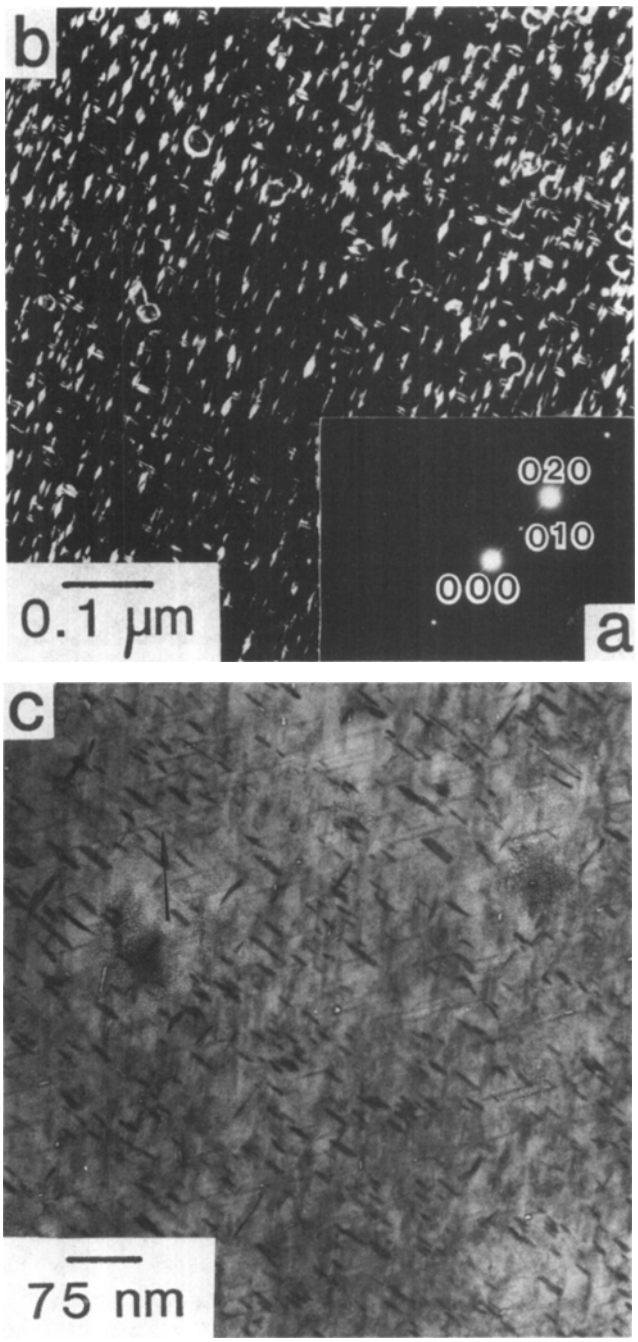

Fig. 2—(*a*) Diffraction pattern of UA-2 showing the Al_3Li-Al_3Zr superlattice spot and the streak corresponding to Al_2Cu precipitates. (*b*) DF image showing the three variants of Al_2Cu precipitates. Note the Al_3Zr dispersoids. (*c*) BF of Θ' and T_1 precipitates in the {112} foil plane in PA.

Many of the Θ' precipitates in one of the variants appear to be more elliptical than normally observed in Al-Cu binary alloys.[14] This may indicate that Al_3Li has nucleated on one of the three variants of the Al_2Cu precipitates. It may also be due to the incorporation of some Li in the Θ'' phase. Silcock[15] has theorized that $Al_{7.5}Cu_4Li$ (T_B) forms continuously from Θ' by the replacement of Al atoms by Li, and Noble *et al.*[16] have shown that Li may cluster with Cu to form plate-shaped zones having a (100) habit plane similar to Θ'. Noble and Thompson[10] also observed that δ' coprecipitated with Θ' and Al_2CuLi (T_1) in an Al-3.5Cu-1.5Li alloy during the aging at 150 °C. No T_1 precipitates were observed for either the UA1 or UA2 conditions, but both Θ' and T_1 were present in the PA condition, Figure 2(c) in our study.

During artificial aging Θ' coarsens and transforms to the equilibrium Θ phase which is incoherent with the matrix. The formation of the Θ phase is normally accompanied by softening in Al-Cu binary alloys. However, for all of the aging conditions used in this study streaks associated with Θ' were present and no Θ diffraction spots were observed in the electron diffraction patterns. Streaks associated with Θ' were still present even after 40 hours at 160 °C (Figure 3(a)), and DF electron micrographs using these streaks revealed the fine, coherent Θ' precipitates (Figure 3(b)). This result is consistent with the results of Noble and Thompson[10] who showed that streaks associated with Θ' were still present in an alloy of similar composition even after aging for one week at 190 °C. After aging for 40 hours at 160 °C, diffraction patterns from the [110] zone contained streaks associated with T_1 (Figure 3(c)), and DF electron micrographs using these streaks revealed thin coherent T_1 precipitates (Figure 3(d)). The coherency of T_1 was verified by the absence of misfit dislocations using bright-field images employing different g vectors in two-beam conditions (Figure 4). Our analysis, along with the results of others[9–11,14,17] suggest that both Θ' and T_1 remain coherent across their habit planes for all of the aging treatments used in this study.

The tensile properties obtained at various aging times are listed in Table II. The peak strength was found to be lower than that of the M2-T651 alloy investigated by Feng *et al.*[7] This is attributed to the lower Cu content in the present alloy and thus a lower volume fraction of the major strengthening precipitates, Θ' and T_1. The slip behavior was studied by TEM analysis of thin foils obtained from regions adjacent to the fracture surface of the tensile samples. Slip bands in {111} type slip planes were chosen and the imaging of the bands was performed using a $\mathbf{g} = \bar{2}20$ or $2\bar{2}0$. Four to five different grains were chosen in each aging condition, and average values of the slip band width and spacing were obtained. Representative micrographs of the slip character obtained with a [110] zone axis show planar slip behavior observed for all the aging conditions employed (Figures 5(a) through (d)). In the as-quenched condition only a few planar slip bands were observed at near fracture strain and only in certain grains as most of the deformation was homogeneously distributed. These slip bands may be associated with some $Al_3Li(\delta')$ (although not observed) or short-range order[18,19] being present in the as-quenched condition. It is observed that with progressive aging the fine relatively homogeneous slip changes to well-defined intense slip bands in the peakaged condition. These bands become more prominent, the separation between them increases, and their width decreases as aging progresses as shown in Figures 6 and 7. It should be noted that the volume fraction of T_1 increases with aging up to the peakaged condition. The slip bands still persist in the slightly overaged condition (Figure 5(d)), due to the presence of semicoherent precipitates. However, they are more diffused when compared to the peakaged condition, suggesting a slight reversal to relatively homogeneous slip. The slip bands are most often continuous across the subgrains.

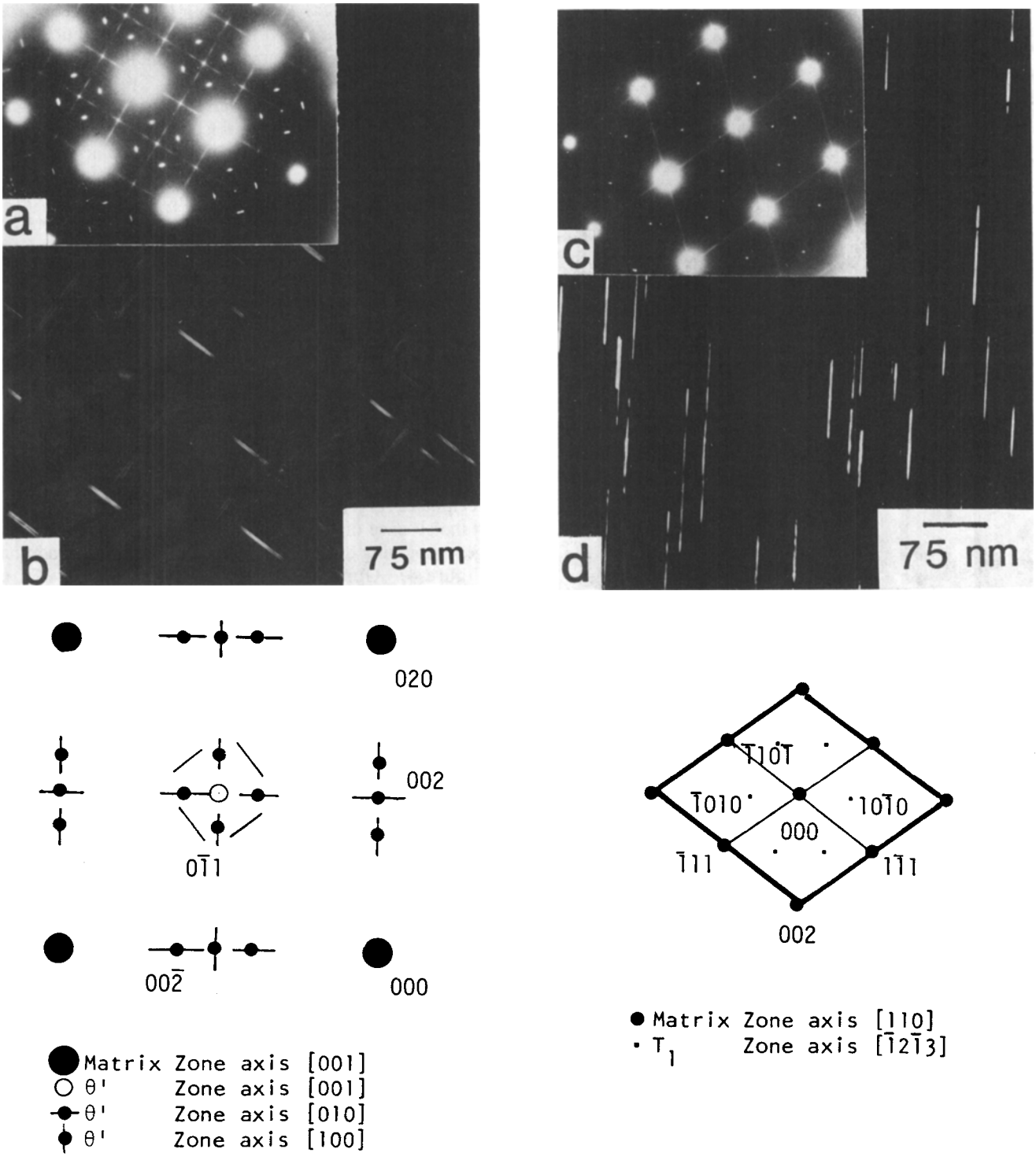

Fig. 3—(*a*) Diffraction pattern with a [100] zone axis, shows the streaks associated with Θ' precipitates. (*b*) DF of Θ' using the streak associated with precipitates lying on the {100} planes of the matrix. (*c*) Diffraction pattern with a [110] zone axis, shows the streaks associated with the T_1 precipitates. (*d*) DF of T_1 using the streak associated with the precipitates lying on the {111} planes of the matrix. Sample aged at 160 °C for 40 h.

The changes in the monotonic properties and slip behavior with aging show that the increase in yield strength is accompanied by increasing amounts of strain localization in the slip bands and a concomitant decrease in the strain hardening exponent and ductility level. The formation of sharp slip bands is a consequence of dislocations shearing the precipitates. When shearing occurs the strengthening effect of the precipitates is reduced, the slip plane weakens, and slip occurs preferentially on these planes.[20,21,22] This results in an inhomogeneous slip distribution which almost always leads to a considerable loss in ductility and macroscopically brittle fracture as particle hardening is increased.[23–26] The tendency for inhomogeneous slip increases drastically with aging time until the deformation mode

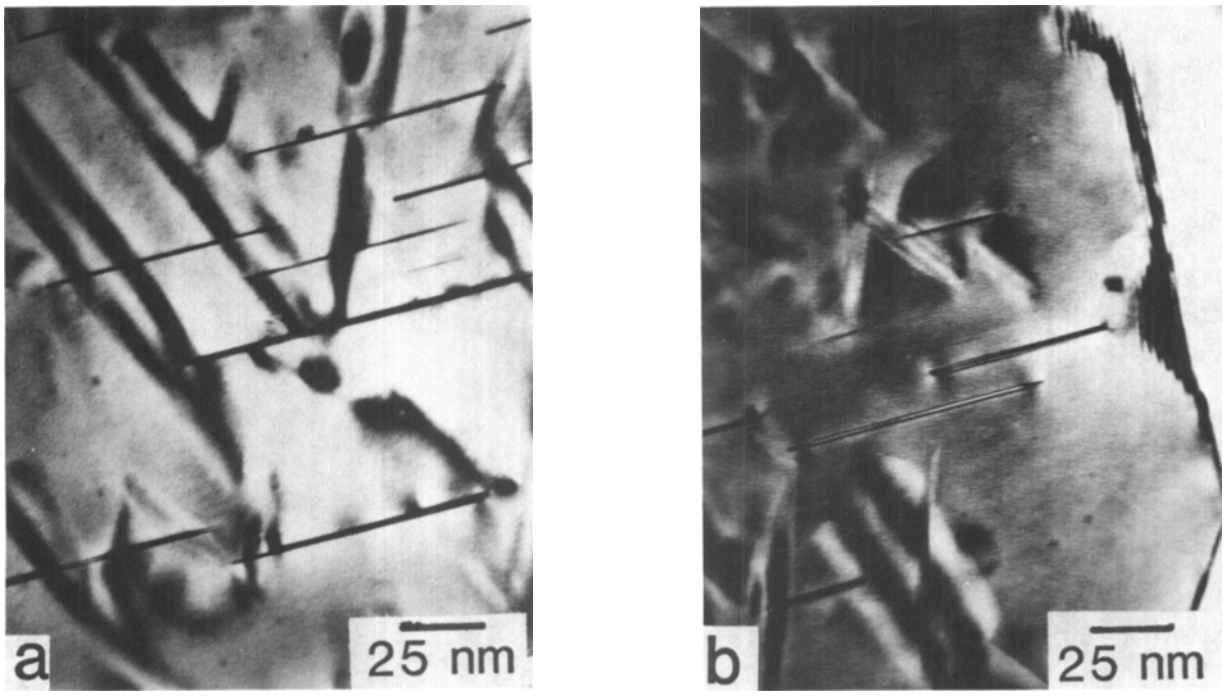

Fig. 4—BF images in the overaged condition with (*a*) $\mathbf{g} = 2\bar{2}0$; (*b*) $\mathbf{g} = \bar{2}20$. Sample aged at 160 °C for 40 h.

changes from dislocation shearing to dislocation looping, at which time the homogeneity of deformation increases. This is easily understood when considering the strengthening associated with shearable particles.

Using, as an example, the model developed by Gleiter and Hornbogen[20,21] for misfit-free, ordered particles (such as Al_3Li), the increase in the critical resolved shear stress, $\Delta\tau_0$, associated with the strengthening precipitates is given by:

$$\Delta\tau_0 = 0.28G^{-1/2}b^{-2}\gamma^{3/2}f^{1/2}r_0^{1/2} \quad [1]$$

where γ is the antiphase boundary energy, G is the shear modulus, b the Burgers vector, f the volume fraction of precipitates, and r their radius. We note that the strength increases with both particle size and volume fraction. Although the particular strengthening mechanism, *i.e.*, coherency hardening, surface hardening, chemical or order hardening, stacking fault hardening, and modulus hardening, may vary among different alloy systems, the strengthening associated with shearable particles always increases with both volume fraction and particle size,[27] similar to the expression developed by Gleiter and Hornbogen. Consequently, the degree of work softening possible during deformation and thus the tendency toward localized slip is proportional to the magnitude of $r^{1/2}f^{1/2}$.[19,24] If one examines the local change in critical resolved shear stress per number of passing dislocations, one observes that the rate of change increases as the volume fraction increases and the particle size decreases.[28] However, for very small particles the absolute change in shear stress is small, so the degree of strain localization is also small.

When the yield strength is exceeded in an age hardened alloy, local softening, equal in magnitude to that associated with the hardening of the shearable precipitates, occurs since the particles are destroyed by the slip dislocations. The dislocations form intense slip bands which impinge upon the grain boundaries. The slip bands are usually not confined to a single slip plane but cover a small volume in which the spacing of the individual active slip planes may be of the order of the atomic spacing.[24] When the local work softening within the slip band is complete, the slip band strain-hardens internally until the stress of the surrounding aged matrix is reached[26] or fracture occurs. Consequently, in microstructures with different degrees of age hardening, the slip bands contain different numbers of dislocations, with the local dislocation density increasing with increasing degree of age hardening, *i.e.*, with $f^{1/2}r^{1/2}$.

The lower degree of strain localization associated with the underaged conditions results in a larger capacity for strain accumulation. This is reflected both by the high strain hardening exponents and strains to fracture. With aging the strain hardening exponent decreases, reaching a minimum in the peakaged condition, due to increased work softening in the slip bands.[27] Since the majority of the deformation is localized, the net effect is a lower ductility level. Beyond the peakaged condition one would expect slip to become more homogeneous since overaging is normally accompanied by a change in deformation mechanism from dislocations shearing particles to dislocations looping and bypassing particles. In actuality, for most aluminum alloys, this transition in deformation mode normally begins before the peak strength is reached as some of the larger strengthening precipitates become incoherent and cannot be sheared. Consequently, for most age hardening aluminum alloys the highest degree of strain localization is observed for a slightly underaged condition. However, Θ' and T_1 phases were observed to maintain their coherency in the peakaged condition for the thermal treatments used in this study and the transition in deformation mode occurs only after overaging. An increase in strain hardening exponent should accompany this change in deformation mode, and this was observed in the present study. However, an increase in strain-to-fracture is not observed in OA-2 and OA-3

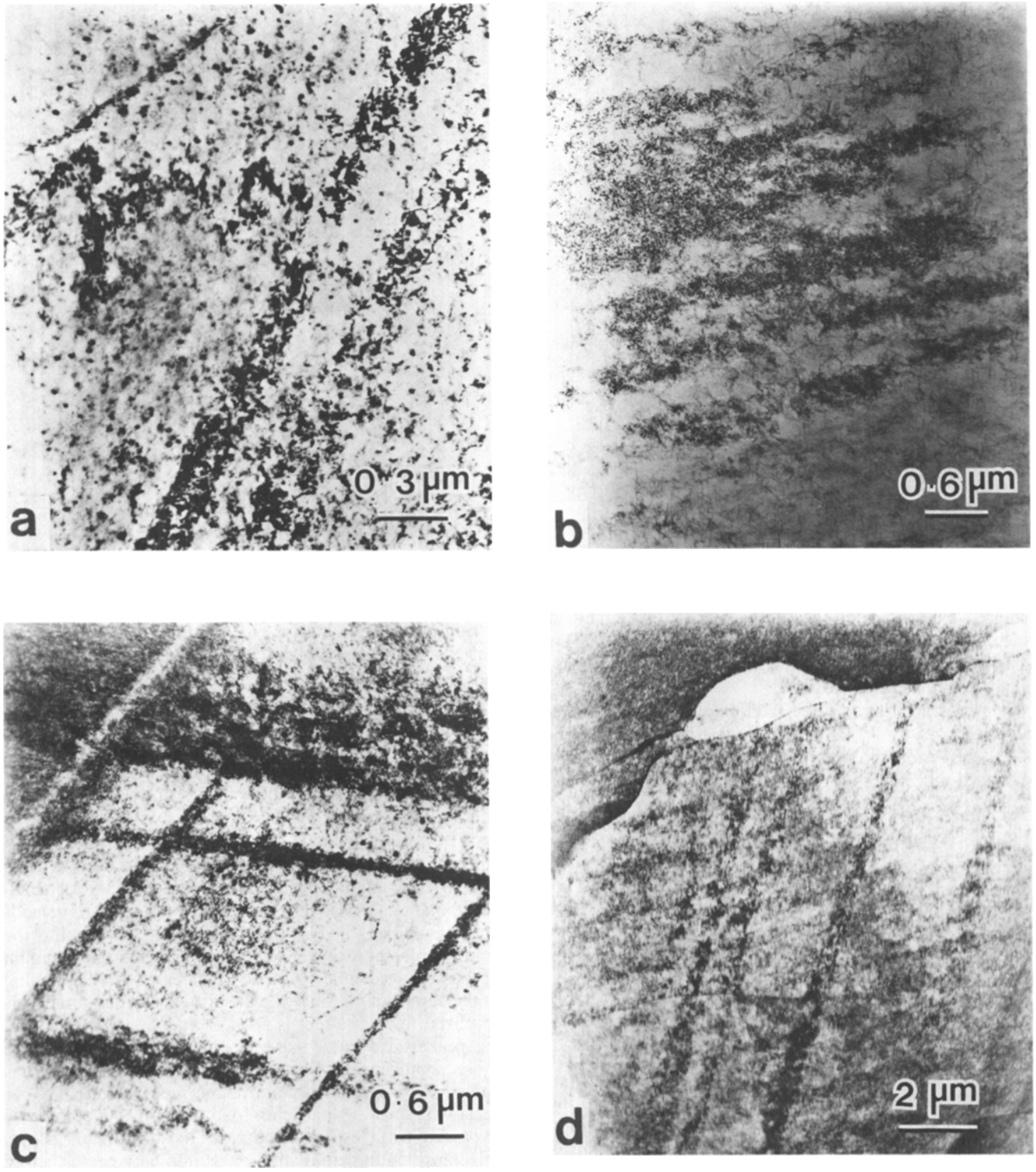

Fig. 5 — Bright-field TEMs with ⟨110⟩ zone axis illustrating the planar slip bands in fractured tensile specimens aged at 434 K for (*a*) 0 h, (*b*) 10 h, (*c*) 17 h, and (*d*) 22 h; $\mathbf{g} = 2\bar{2}0$.

(Table II), because the equilibrium precipitates that form at grain boundaries during overaging, and the associated precipitate-free-zones, aid the void nucleation and coalescence. Transmission electron micrographs of OA-2 (Figure 5(d)) showed that planar slip persisted in the overaged condition, although the deformation was more homogeneous than that observed for the PA condition. This is not surprising since both Θ' and T_1 were observed to maintain coherent interfaces with the matrix across their habit planes, for all aging conditions studied, and may continue to be sheared even though the drop in yield strength for OA-1, 2, and 3 indicated that some particles should be bypassed by

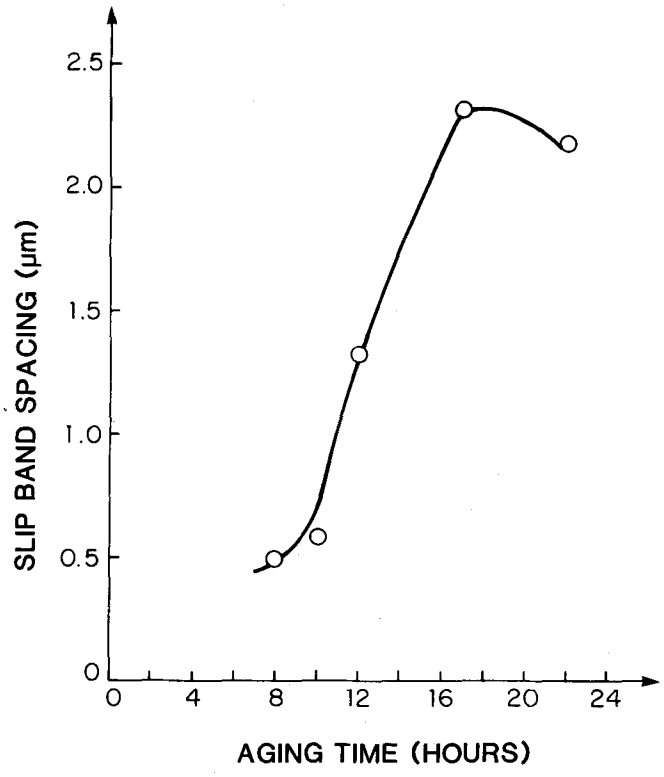

Fig. 6—Variation of slip band spacing with aging time.

dislocations. An alternative explanation for the drop in yield strength is that there is a decrease in the volume fraction of strengthening precipitates associated with the precipitation of the equilibrium phases at grain boundaries in the late stages of aging. The shearing of T_1 was observed in DF TEM's of an OA-2 tensile sample that had been given 2 pct plastic strain (Figure 8).

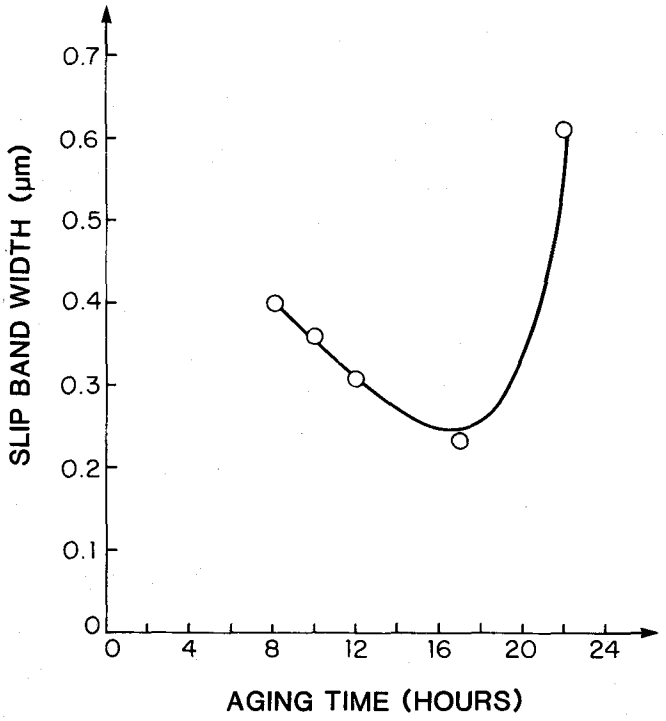

Fig. 7—Variation of slip band width with aging time.

The effect of slip localization on the tensile fracture can be observed in the fractographs (Figure 9) for an underaged and overaged alloy. In both cases transgranular shear fracture is observed along with some voids associated with precipitate particles and/or slip band intersections. There was little evidence of intersubgranular fracture although secondary cracking was observed along the high angle grain boundaries of the overaged sample (Figure 9(b)). This intense secondary cracking may be associated with the small recrystallized grains observed in Figure 1(a), but is most likely due to the presence of coarse equilibrium precipitates at the high angle grain boundaries and the presence of a PFZ adjacent to the boundary. The decrease in ductility with aging seems to be due simply to the extensive shear localization and accompanying slip band softening up to the peakaged condition. Beyond the peakaged condition larger equilibrium precipitates on the grain boundaries give rise to intergranular cracking which further reduces the ductility.

B. *Near Threshold Fatigue Crack Propagation*

The results obtained from the fatigue crack growth tests in air (R.H. 45 pct) and in vacuum ($<10^{-5}$ torr) are shown in Figures 10(a) and (b) as plots of crack propagation rates da/dN *vs* the stress intensity factor range ΔK. The near threshold fatigue crack growth rates increased and the threshold stress intensities (Table III) decreased with aging in both air and vacuum. Furthermore, there is an enhancement of the fatigue crack growth resistance in vacuum for similar aging conditions. The crack closure data obtained from the compliance *vs* load curves has been expressed[29] in the form of the closure stress intensity factor $\Delta K_{th}^{Cl} = K_{th}^{Cl} - K_{th}^{\min}$, and the intrinsic (or effective) stress intensity factor $\Delta K_{th}^{i} = \Delta K_{th}^{obs} - \Delta K_{th}^{Cl}$, as shown in Table III. These values indicate that the intrinsic fatigue crack growth thresholds follow the same trend as the apparent or observed values, for the aging conditions tested here.

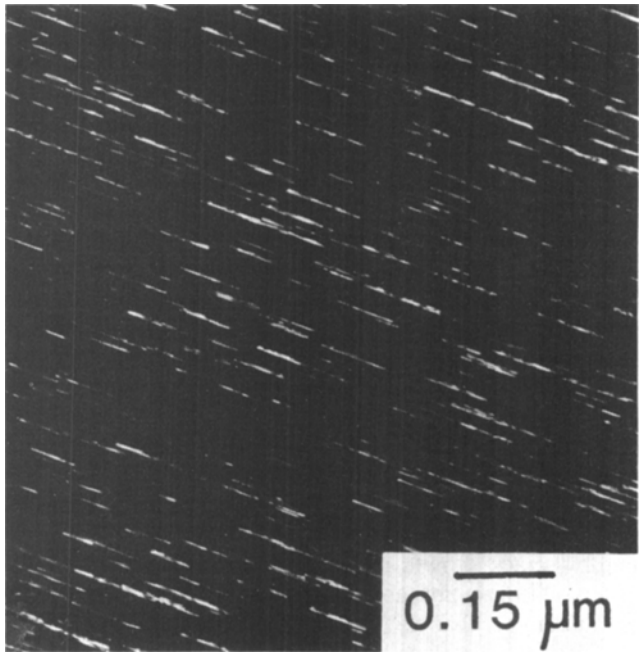

Fig. 8—DF micrograph showing the T_1 shearing in OA-2 imaged with the T_1 streak, zone axis near [110].

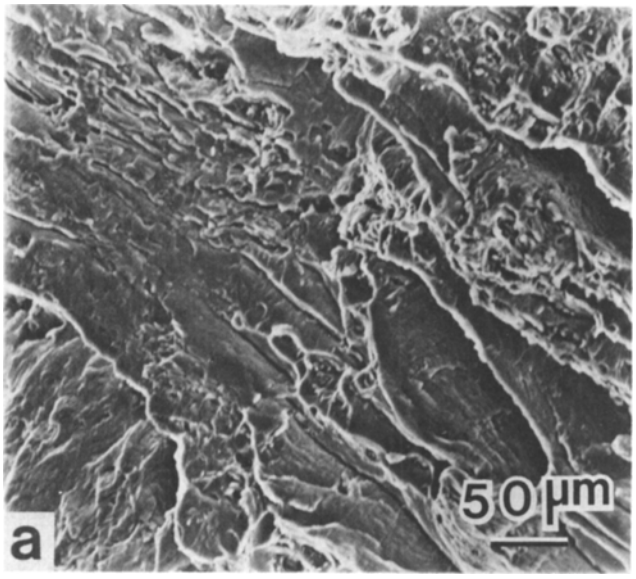

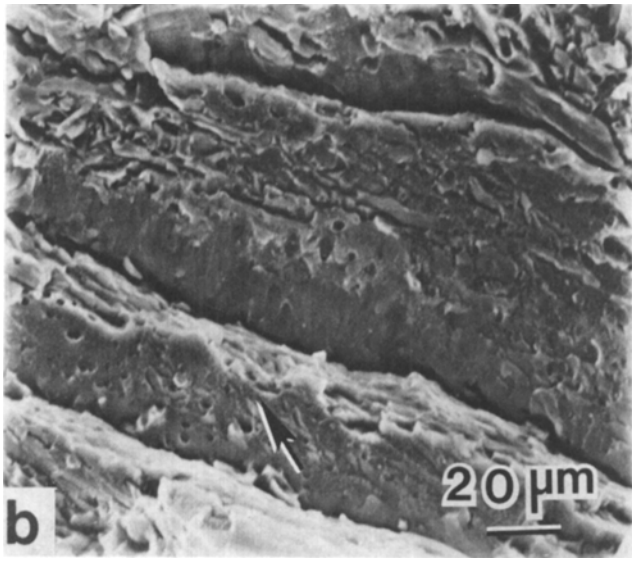

Fig. 9—SEM micrographs of the transgranular shear fracture in tensile testing: (*a*) underaged conditions and (*b*) overaged conditions. Secondary cracking and voids associated with equilibrium precipitates (shown by arrow) are observed in condition (b).

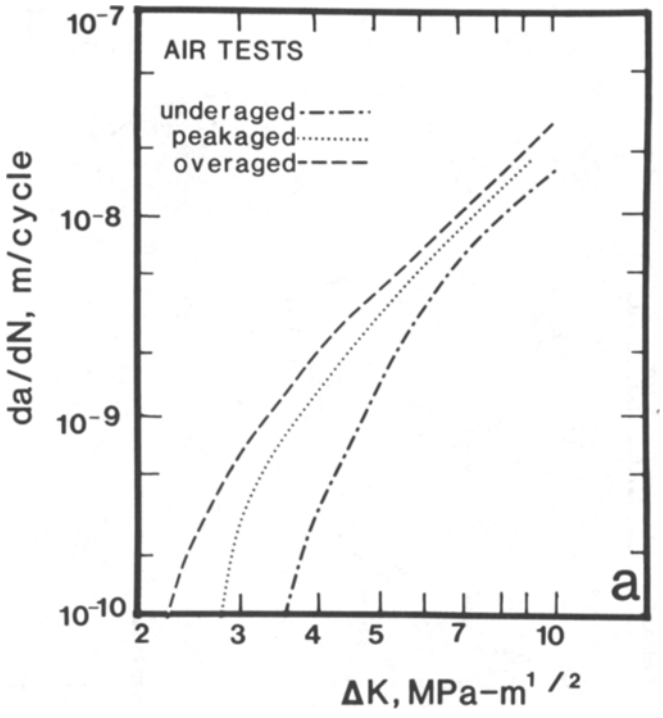

(*a*)

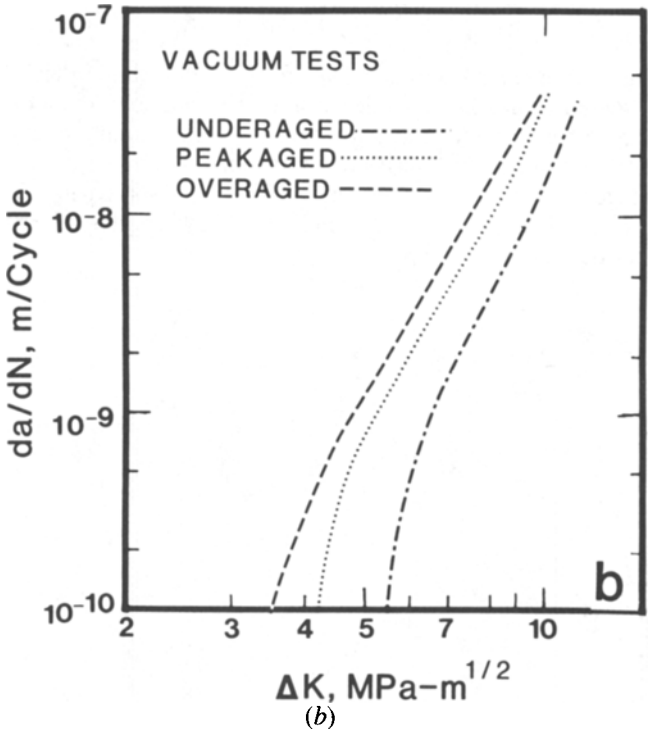

(*b*)

Fig. 10—Fatigue crack growth rates of the microstructural variants tested in (*a*) laboratory air (R.H. of 45 pct) and (*b*) vacuum (10^{-5} torr).

Figure 11 shows the crack paths for the alloy tested in air in the under and overaged conditions. The observed deflections appear to be due to the crack propagating along the slip bands. It is not surprising that extensive crack deflections also occurred in the overaged alloy since slip planarity is maintained and intense slip bands are available for crack propagation paths. Suresh and Vasudévan have also observed[30] equal degrees of crack deflections in under- and overaged conditions in low Li containing alloys.

The fracture surface features shown in Figure 12 reveal that the mode of crack growth is highly crystallographic in the low crack growth rate region. Extensive faceting was observed in vacuum, and the fracture surfaces were considerably rougher than those observed on the samples tested in air. The lower crack path tortuosity in air as compared to that in vacuum could be due to the aggressive air environment reducing the amount of irreversible plasticity needed for the crack to propagate.[31] There is the possibility for oxide formation which might be expected to enhance closure, thus giving an apparent higher threshold. However, Vasudévan *et al.*[32] showed by SIMS that the thickness of the oxide for a similar alloy 2020 is considerably smaller than the crack opening displacement, suggesting that the oxide contribution, if any, would be negligible.

Table III. Fatigue Threshold Stress Intensities

Microstructure	Environment	ΔK_{th}, MPa $m^{1/2}$	ΔK_{th}^{i}, MPa $m^{1/2}$	ΔK_{th}^{Cl}, MPa $m^{1/2}$
UA-2	air	3.7	3.1	0.6
PA	air	2.8	2.4	0.4
OA-2	air	2.3	2.3	negligible
UA-2	vacuum	5.5	5.3	0.2
PA	vacuum	4.3	4.0	0.3
OA-2	vacuum	3.6	3.4	0.2

$\Delta K_{th} = \Delta K_{th}^{observed}$ or $\Delta K_{th}^{apparent}$
$\Delta K_{th}^{i} = \Delta K_{th} - \Delta K_{th}^{Cl}$
$\Delta K_{th}^{Cl} = K_{th}^{Cl} - K_{th}^{min}$

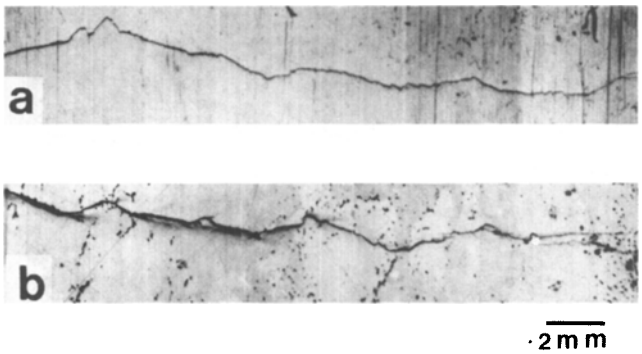

Fig. 11—Optical micrographs of the crack profile of the fatigue crack propagation samples tested in air: (*a*) underaged condition and (*b*) overaged condition.

Figure 13 compares the results obtained for the Al-Cu-Li alloy with those of a thermomechanically processed 7475.[33] The fatigue crack growth rates and thresholds of the Al-Cu-Li alloy are better than those of the 80 μm grain size 7475. Several investigators have proposed that the fatigue crack growth rates decrease with increasing modulus,[34] thus indirectly predicting that Li-containing Al alloys would have improved FCP resistance. Therefore, a more realistic comparison of the two materials may be obtained by normalizing the stress intensity range with Young's modulus since the yield stresses are approximately the same. As shown in the normalized curves of Figure 13(b), the fatigue growth rate curves remain below the 7475 alloy suggesting that the improvement is not due to the modulus effect alone. In a similar comparison, Vasudévan *et al.*[32] came to the conclusion that the crack deflections in the 2020 alloy were a major cause for improved crack growth resistance over that of a 7075 alloy. A comparison of the crack deflections observed in 7475[33] with those observed here also shows that this mechanism may account for the improved crack growth resistance observed, although differences in slip reversibility may also be a contributing factor.

In the present alloy the crack propagation rates are higher in the overaged condition as compared to the peak- and underaged conditions. These observations are consistent with earlier observations made by other investigators in age hardened systems.[33,35,36] In these alloys, the dislocations shear the coherent precipitates and thus promote inhomogeneous slip in the under- and peakaged conditions. In the overaged alloys, the coherency between the precipitates and matrix is reduced (although not lost), resulting in less heterogeneous slip as discussed before. The dislocations emitted from the crack tip move forward on the slip plane in the rising half of the fatigue cycle. In the under- and peakaged conditions the fraction of the dislocations that move back is larger compared to the overaged condition since the particles are more easily cut in the former case and large numbers of dislocations are not required to destroy the strengthening effect of the particles. In other words, the slip reversibility would be higher in the under- and peakaged alloy and the plastic strain accumulation would be lower for a given number of cycles. For the overaged alloys, the slip reversibility is reduced because of the larger precipitates and because the precipitate bypass mechanism is also active. This leads to a higher accumulation of plastic strain in the OA alloys for the same number of cycles and implies that for a given ΔK an overaged material would exhibit faster crack growth rates compared with lower aging conditions. A similar argument can be presented for the peakaged alloy when compared to the underaged, *i.e.*, the strengthening precipitates are larger, they require a larger number of dislocations to destroy their strengthening effect, so slip reversibility is less than for the underaged alloy; especially at low stress intensities.

Slip reversibility differences appear to be the only logical explanation for observed difference in fatigue crack growth rates between the underaged and peakaged conditions. The trend of the fatigue crack growth rates in vacuum—where environmental effects are minimum—is similar to that in air suggesting that environmental degradation of crack growth resistance[38,39] in maximum slip planarity conditions is not the cause of the observed difference among the three aging conditions. However, a number of significant points should be noted about the vacuum data: (i) closure levels as compared to air decreased, (ii) crack path tortuosity and hence crack deflections increased as compared to that in air, and (iii) fracture surface roughness increased. However, no significant differences of these factors exist among the different aging conditions. As mentioned before, the role of oxide even in air is minimal and therefore the reduction in closure due to oxide asperities in vacuum need not be considered. The other possibility could be due to fracture surface roughness. The results show that the fracture surface roughness increases considerably in vacuum with a concomitant decrease in crack closure. This suggests that the mode II displacements[40] produced due to crack path tortuosity in vacuum are reduced, or more reversible, giving rise to lower closure levels. For the 7475 alloy tested in vacuum, Carter *et al.*[33] showed that in spite of a major difference in the crack deflections and crack path tortuosity among the aging conditions and in different environments,

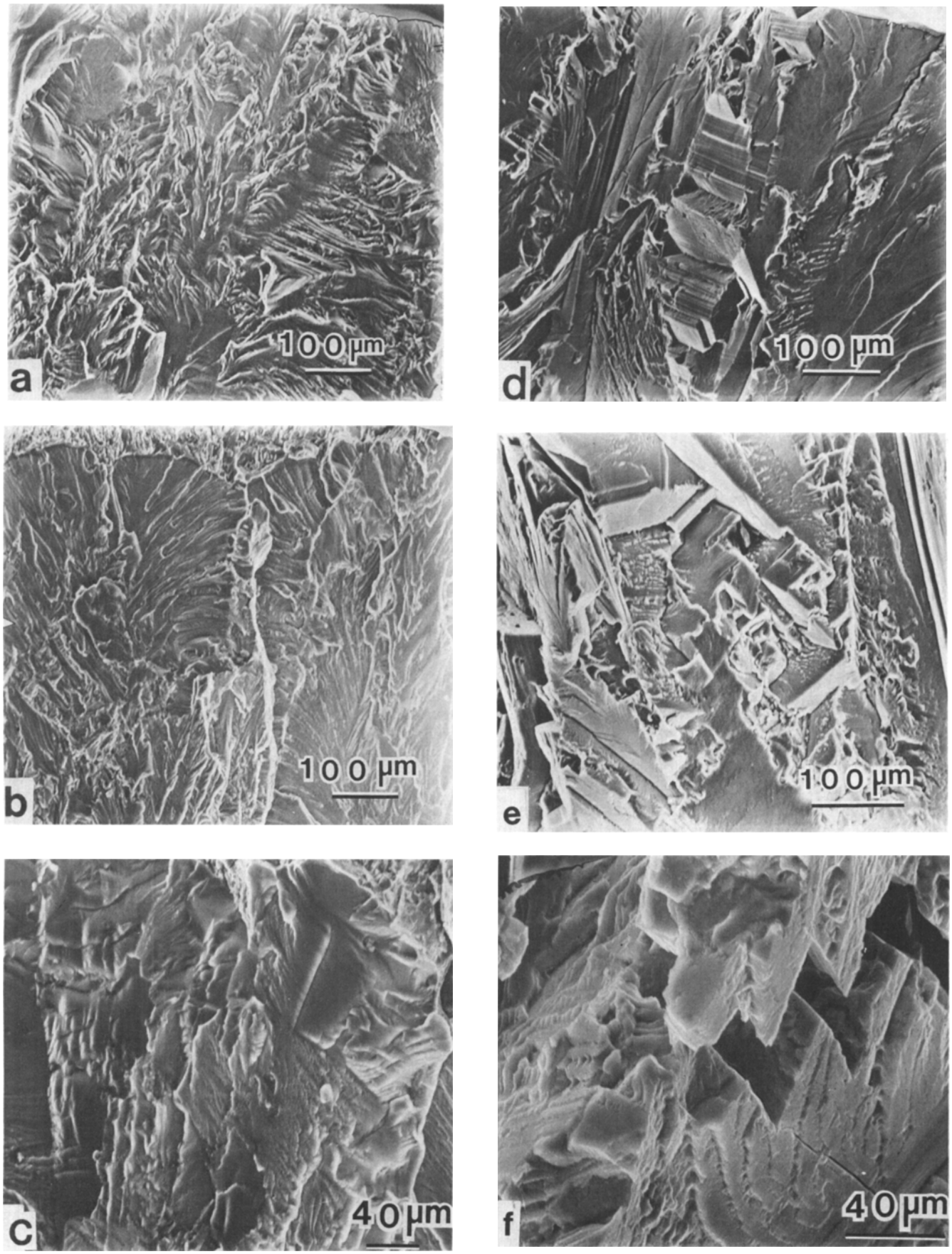

Fig. 12—Fractography associated with fatigue crack propagation near threshold: (*a*) UA-2 tested in air, (*b*) peakaged tested in air, (*c*) OA-2 tested in air, (*d*) UA-2 tested in vacuum, (*e*) PA tested in vacuum, and (*f*) OA-2 tested in vacuum.

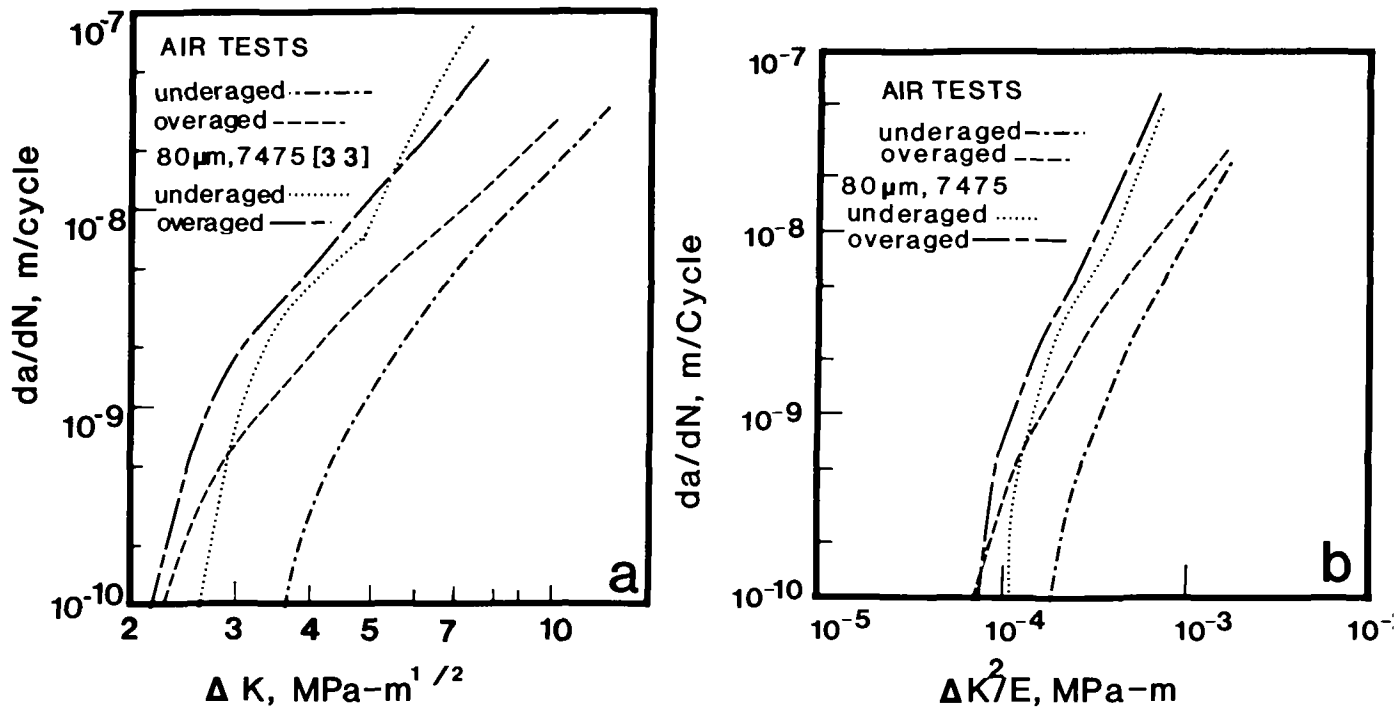

(*a*) (*b*)

Fig. 13 — A comparison of the fatigue crack growth rates of the present alloy with thermomechanically processed 7475 alloy as a function of (*a*) ΔK and (*b*) as a function of normalized ΔK^2 with respect to Young's modulus E.

the contribution from the geometrical effect of crack deflections[37] could only partially account for the differences in crack growth resistance. They suggested, as had others,[33,35,36] that the extent of slip reversibility plays an important role in the fatigue crack growth rates of planar slip materials. In a vacuum environment, the slip reversibility increases due to the lack of a significant surface oxide. Thus although fractography of vacuum tested samples indicates extensive faceting, it does not result in an increase of ΔK_{th}^{Cl}. The effects of mode II displacements behind the crack tip appear to be reduced in vacuum due to improved slip reversibility. Thus, not only the ΔK_{th}^{Cl} is decreased, but also the intrinsic crack growth resistance ΔK_{th}^{i} is increased in vacuum.

C. *Fracture Toughness*

One of the major goals in the development of Al-Li alloys has been to develop microstructures capable of exhibiting fracture toughness levels comparable to the 7XXX series and improvements in strength, modulus, and density over the existing 2XXX alloys. Although several investigations have addressed the ductility problems of these alloys, very few have concentrated on the problem of fracture toughness.[7,41,42] Previous investigations[3] on the fracture behavior of the Al-Li-X alloys have shown that strain localization curtails ductility in the peakaged condition. Strain localization, in conjunction with large equilibrium precipitates along boundaries, promotes intergranular/intersubgranular fracture associated with wide PFZ's. Efforts to decrease the formation of the PFZ's have included chemistry modifications and deformation prior to aging. The latter process involves the introduction of dislocations which serve as sites for those precipitates that have a large coherency strain field, *e.g.*, Θ' and T_1. Recent studies by Feng *et al.*[7] on Al-Li-Cu alloys have shown that in the presence of Cd, deformation prior to aging might not be necessary to obtain a uniform and dense precipitation of the Θ' and T_1 phases. Another beneficial effect of Cd is to slow down the growth kinetics of the strengthening precipitates by segregating to the Θ'-matrix interfaces and reducing the interfacial energy.[43,44] However, excessive amounts of Cd may segregate to the grain boundaries and contribute to the intergranular fracture.[8]

Recrystallized and partially recrystallized structures may also be detrimental to ductility when compared with unrecrystallized structures due to secondary crack paths along the recrystallized grains.[8] The suppression of recrystallization in aluminum alloys is normally attained by adding dispersoid forming elements, Cr or Mn or Zr. Of these, Zr has been observed to be the most potent in suppressing recrystallization.[45] The improvement in the fracture toughness observed when adding Zr has been associated with a lesser degree of secondary cracking along the recrystallized grains.[45] However, it may also be associated with the small particle size and coherent interface when compared with Cr and Mn dispersoids. In the present work we have concentrated on the effect of the slip process on the fracture toughness. The slip process is undoubtedly controlled by the strengthening precipitates, but eventually the slip dictates the fracture toughness in Al-Li-X alloys as discussed below.

The fracture toughness data collected over a wide range of aging times from compact tension specimens are summarized in Table II. The results show decreasing fracture toughness with aging, typical of many other aluminum alloys such as 2020.[46] The accompanying change of yield

stress with aging (Figure 14) shows that the K_{1C} decreases as the yield stress increases until the peakaged condition is attained beyond which the strength-toughness combination decreases. A comparison of the K_{1c} values of this alloy to the commercial 2020 alloy containing Cu, Li, Mn, and Cd (Figure 14) shows that the toughness levels are comparable only at the lower aging conditions, whereas for longer aging the present alloy retains high toughness. For example, at a strength level of 475 MPa, the K_{1c} values are 35 and 20 MPa-$m^{1/2}$ for the present alloy and the commercial 2020 alloy, respectively. In the same Figure, K_{1c} values recently obtained for an Al-2Li-4Mg alloy[46] and a modified 2020 alloy[7] are also shown for comparison purposes.

The other mechanical property data show that the decreasing fracture toughness is accompanied by a decrease in the strain hardening exponent and strain to fracture suggesting the possible role of these variables on the fracture toughness, as will be discussed later. Extensive fractography of the fracture toughness samples revealed transgranular slip band fracture and secondary cracking along grain boundaries, in both under- and peakaged (Figures 15(a) and (b)), some very rare occurrence of transgranular microvoid coalescence (Figure 15(c)), and ductile intergranular failure in the overaged microstructure (Figure 15(d)).

The major transgranular slip band fracture mechanism in the underaged to peakaged conditions was found to occur over several microns ahead of the crack tip. These observations suggest that the slip bands emanating from the crack tip have often extended unimpeded transgranularly across many subgrains and possibly several grains. This is due to the low misorientation between subgrains and the sharp deformation texture of the plate. Some transgranular microvoid coalescence associated with iron and silicon constituents as shown in the micrograph of Figure 15(c) was rare and did not appear to control the overall fracture. The major mechanism of fracture for the overaged conditions

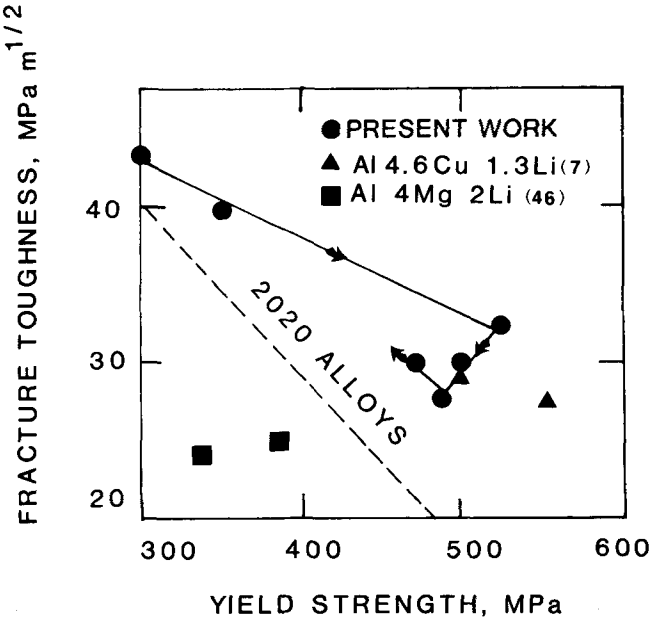

Fig. 14 — Variation of fracture toughness with yield strength for the present alloy and a comparison to the data of other Al-Li-X alloys.

(Figure 15(d)) shows the presence of small microvoids along grain boundaries suggesting a ductile intergranular type of failure, associated with a weakening of the grain boundaries in the overaged conditions. Starke, Sanders, and Palmer[3] suggest that for Al-Li alloys the slip bands impinging on the grain boundaries transfer the strain to the soft PFZ's along the grain boundaries. These regions deform with ease and hence strain is localized here, giving rise to a more easily attainable fracture route along the grain boundaries.

Many investigations in the past have shown that a relationship between the strain hardening exponent obtained in uniaxial tension tests and K_{1c} exists.[47,48,49] Recently, Garret and Knott[47] have shown that the critical crack opening displacement at the onset of crack extension is proportional to the square of the strain hardening exponent for a constant ductile fracture strain, thus suggesting that the K_{1c} is proportional to the strain hardening exponent. The dependence of K_{1c} on the strain hardening exponent for the Al-Cu-Li alloy under study is suggested by the micrographs of Figure 16, taken after unloading the compact tension samples at the onset of crack extension. These micrographs illustrate that, in the underaged condition, the plastic zone wings are wider than in the peakaged condition. Gerberich[50] and Hahn and Rosenfield[51] showed for a number of alloy systems, including aluminum alloys, that the plastic zone width, D, is proportional to the square of the strain hardening exponent, n, given as

$$D(n) = 0.0013 + 2.54n^2(\text{cm}) \qquad [2]$$

Due to the dispersion of the plasticity, the crack tip in the underaged condition experiences a lower strain concentration than in the peakaged condition for a given load level (Table IV). Thus the load bearing capacity in the presence of a notch is higher in the underaged conditions. If the crack extension is considered to occur after a critical strain has accumulated or when the strain hardening capacity is exhausted, then the underaged samples would exhibit a higher fracture toughness.

This qualitative relationship between the fracture toughness and the strain hardening exponent does not, however, offer an explanation at a microscopic level, since the plastic zones in front of the crack tip include the plasticity in intense slip bands as well as the plasticity between the bands. In order to incorporate microstructural features and the process zone, it might be necessary to consider the extent of strain localization which is controlled by the character of the strengthening precipitates.

Going from the underaged to peakaged condition, the fracture toughness is limited by the slip band decohesion process without the involvement of any void growth. This process is considered to occur when a critical displacement or strain is reached in some potential slip bands in front of the crack tip. A similar criterion has been discussed in detail by Smith, Cook, and Rau[52] for materials exhibiting strain localization. The analysis here is different in that the macroscopic shear fracture is related to the local plasticity in the slip bands where the degree of localized plasticity as observed increases with degree of aging till the peakage condition is reached.

We have approached this problem by considering slip on planes inclined to the crack plane at an angle α.[53,54] In such a situation the vertical displacements in two symmetric slip

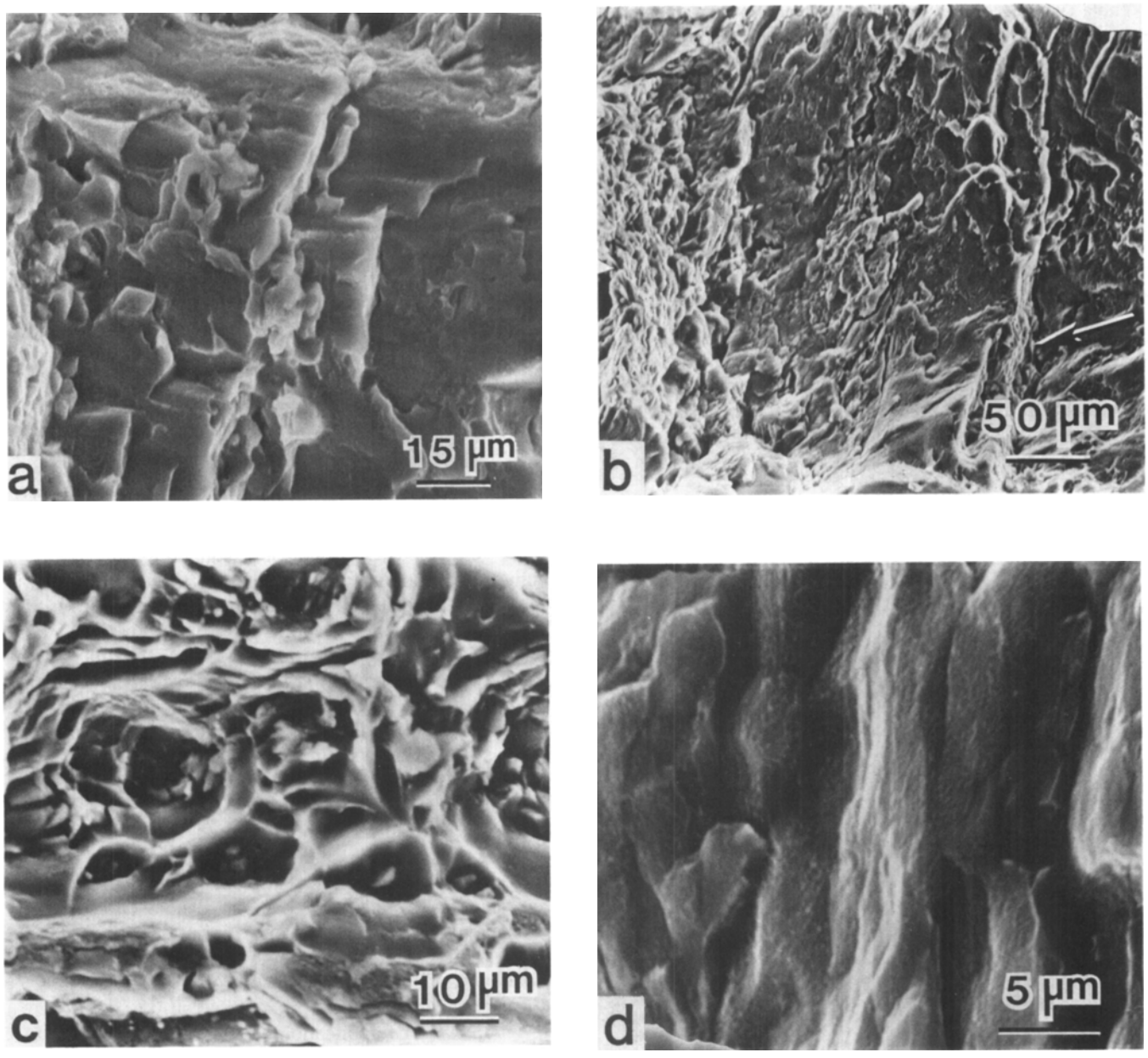

Fig. 15—SEM micrographs of the fracture features in fracture toughness samples illustrating slip band fracture and secondary cracking (shown by arrow) in (*a*), UA-2 and (*b*) PA, microstructures, (*c*) rare occurrence of voids initiated at constituent particles, PA, and (*d*) ductile intergranular and ductile intersubgranular fracture in OA-2.

bands produced by N dislocations in front of the crack tip having similar Burgers vector b would be $2(Nb)$ Sin α. This displacement in the front of the crack tip would then be accommodated by the vertical crack tip opening displacement, δ, leading to

$$\delta = 2(Nb) \text{ Sin } \alpha \qquad [3]$$

The dislocations in front of the crack tip may be homogeneously distributed throughout the plastic zone, and some may be concentrated in intense slip bands that lie within the plastic zone. Consequently, δ may be the sum of these contributions

$$\delta = 2[(N)_u b + (N)_{SB} b] \text{ Sin } \alpha \qquad [4]$$

where $(N)_u b$ represents the displacement due to homogeneous slip and $(N)_{SB} b$ represents the displacement in the slip bands. The relative magnitude of each contribution would be dependent on the aging conditions since the tendency for strain localization increases as aging progresses up to the peakaged condition. Only those dislocations in the intense slip bands should be considered to contribute to the critical strain that is necessary for transgranular slip band fracture. The density of these dislocations may be defined as

$$\rho_{SB} = (N)_{SB}/LW \qquad [5]$$

where W is the slip band width and L the slip band length. Following Orowan, the shear strain in the slip band may be written as

Table IV. Measured Values of Deformation Parameters

Microstructure	Slip Band Width W (μm)	Slip Band Spacing d (μm)	Plastic Zone Width D (μm)
UA-1	0.4	0.5	442
UA-2	0.31	1.33	256
PA	0.236	2.316	90
OA-2	0.61	2.166	—

$$\gamma_{SB} = \rho_{SB} bL = \frac{(N)_{SB}}{LW} \cdot bL = (N)_{SB} b/W \qquad [6]$$

A critical value of γ_{SB} would be necessary for fracture to occur. As aging progresses, a smaller δ is required to reach the critical strain since, for a given δ, $(N)_{SB}$ increases and W decreases with aging. We may express δ in terms of the stress intensity factor, K, the yield stress, σ_{ys}, and Young's modulus, E, by the relationship[55]

$$\delta = \frac{0.5K^2}{E\sigma_{ys}} \qquad [7]$$

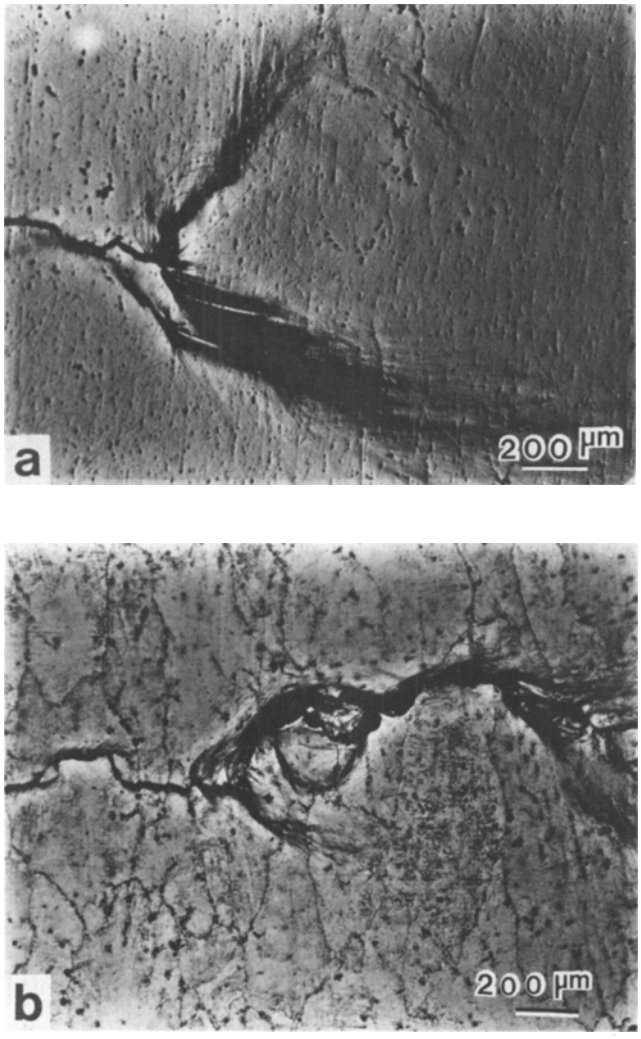

Fig. 16—Optical micrographs comparing the plastic zones, taken after unloading at the onset of initial crack extension in (*a*) underaged and (*b*) peakaged conditions.

Substituting for δ and ignoring the contributions of those dislocations that are homogeneously distributed, we obtain

$$\frac{0.5K^2}{E\sigma_{ys}} = (2 \text{ Sin } \alpha \gamma_{SB} W) \qquad [8]$$

Initial crack extension occurs when γ_{SB} reaches a critical value, γ^c_{SB}, and the fracture toughness may be expressed as

$$K_{1c} = [4E\sigma_{ys}\gamma^c_{SB} W \text{ Sin } \alpha]^{1/2} \qquad [9]$$

This equation has been obtained for two symmetric slip bands at the crack tip. However, the equation needs to be modified to take into consideration the number of active slip bands which would be determined by the plastic zone width (D) and the slip band spacing (d). The modified equation then reads as

$$K_{1c} = \left[8 \text{ Sin } \alpha E\sigma_{ys} W \left(\frac{D}{d}\right) \gamma^c_{SB}\right]^{1/2} \qquad [10]$$

The value of D/d in the peakaged condition from measurements of slip band spacing and etched plastic zone width comes out to be 39. Measured values for other aging conditions were employed in the above equation. The number of active slip bands in front of the crack tip decreases due to higher strain localization as aging increases. The critical strain for fracture was assumed to be either ⅓ (plane strain) or ½ (plane stress) of the tensile fracture ductility of the as-quenched specimen, 0.46. The rationale behind this, is that the loss in ductility and fracture toughness in aged specimens is due to the attainment of the same strain as that of the as-quenched specimen but in localized slip bands. So, with increasing degree of flow localization the same strain is concentrated in lesser number of slip bands causing fracture to be attained earlier than when the slip is not so localized. The factors ½ and ⅓ are taken from Hahn and Rosenfield[51] which essentially account for the plane strain and plane stress ductility situations in notched specimens.

The model predicts the correct trend of the fracture toughness variation with yield strength (Figure 17). Experimental fracture toughness values of an Al-2.1Li-2.9Cu-0.12Zr alloy, obtained by Vasudévan and Suresh,[42] are also shown in Figure 17. The application of the present model to their fracture toughness data is justified based on the similarity in composition and deformation mode with our alloy. Calcu-

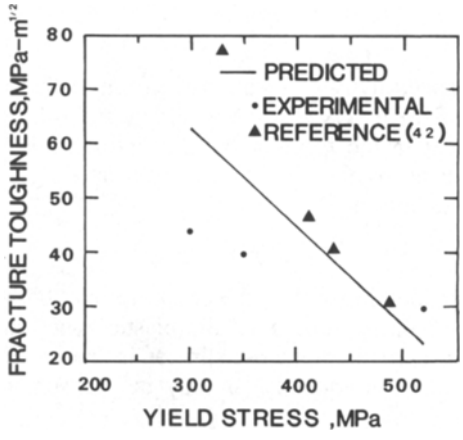

Fig. 17—A comparison of the predicted fracture toughness values to the experimental values.

lated slip band spacings from Vasudévan and Suresh's micrographs for their UA-1, PA, and OA-1 are 3.12, 6.7, and 3.17 microns, respectively, suggesting increasing slip localization from underaged to peakaged and then a return to less localized slip in the overaged condition, similar to the trend we observed (Figure 6). The width of their slip bands could not be measured with accuracy because of the orientation of the sample and the limited resolution of their scanning electron micrographs. As confirmed by our experimental observations and those of Dowling and Martin[58] and Evensen *et al.*,[59] increasing slip band spacing is accompanied by decreasing slip band widths in aluminum alloys (coarse slip refers to small slip band width). We can therefore assume that the slip band width would be a minimum in the peakaged condition of their alloy based on the above findings and also on their observation that the coarsest slip was observed for the peakaged condition. Further evidence of the similarities in the deformation mode of the two alloys is exemplified by the trend in yield stress, strain hardening exponent, and fracture ductility values, with aging.[42] Our model is based on deformation mode (slip band spacing and width), and since similarities in the slip process between two alloys exist, it is appropriate to make a comparison of their fracture toughness values to the predictions of our model for their underaged alloys for which crack extension occurs by transgranular slip band fracture. The higher aging temperature used in their study most likely resulted in extensive grain boundary precipitation in the peakaged condition.[60] This enhanced grain boundary fracture and it was, therefore, inappropriate to compare their peakaged fracture toughness value to the prediction of our model since the model is concerned with transgranular fracture along slip bands. The present analysis suggests that the fracture toughness decreases with increasing yield strength due to a decreasing slip band width and increasing slip band spacing. This is shown schematically in Figure 18. The predicted values are slightly lower at peakaged and higher in the underaged microstructures (Figure 17).

Several investigators[56,57] have examined the problem of ductile fracture strain under different states of stress. Such experiments are currently underway to obtain a better correlation between the slip band width and spacing to the fracture strains in notched tensile specimens.

The behavior of the newly developed Al-Li-X alloys is different from most other aluminum alloys in that the characteristic fracture associated with void initiation at constituent particles and coarse incoherent Mn and Cr dispersoids and the subsequent void growth by shear localization is absent. The volume fraction and size of these particles is low due to the extremely low contents of Fe and Si (Table I) and the use of Zr as the dispersoid forming element. Previous work[7] on Al-Li-Cu alloys containing higher Fe and Si contents suggests that coarse constituent particles aid in fracture initiation *via* microvoid nucleation at these particles and decrease ductility. The Cr and Mn dispersoids may homogenize slip in aluminum alloys and thus increase the work hardening exponent. However, the detrimental nature of the large Mn and Cr containing particles on the fracture ductility is clearly demonstrated in the literature.[45] Microvoids are normally not associated with the small coherent Al_3Zr dispersoids.

IV. CONCLUSIONS

The Al-Li-Cu alloy studied exhibits comparable strength and ductility levels to commercial high strength Al alloys. The yield strength in the peakaged condition is 520 MPa and is accompanied by an 8 pct elongation. The strength increase is, however, accompanied by strain localization which curtails ductility. The general trend of increasing fatigue crack growth resistance with lower aging time remains after considering both crack closure and crack deflections. The fracture toughness in the peakaged condition is 32 MPa $m^{1/2}$. This value together with yield strength compares well with the currently available data on 2XXX and 7XXX alloys. It has been demonstrated that increasing slip localization accompanied by decreasing strain hardening exponent results in a decreasing fracture toughness through a critical strain accumulation at the crack tip needed for the initial crack extension.

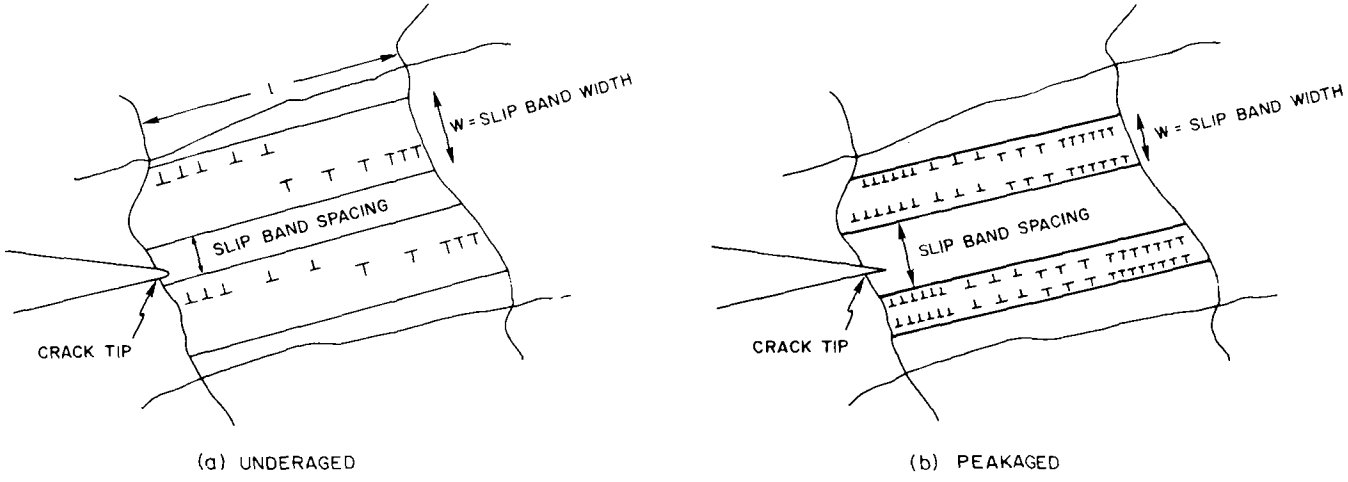

Fig. 18 — A schematic illustrating that the slip bands developed in front of the crack tip are wider and closed spaced in (*a*) underaged conditions due to less heterogeneous slip character and (*b*) narrower and widely spaced in the peakaged condition, due to more localized slip.

ACKNOWLEDGMENTS

This research was sponsored by the Air Force Office of Scientific Research, United States Air Force Systems Command, under Grant AFOSR-83-0061, Dr. Alan Rosenstein, program manager. The authors would like to thank Professor K. Lawless and Mr. W. Cassada for valuable discussions and experimental assistance.

REFERENCES

1. J. S. Ekvall, J. E. Rhodes, and G. G. Wald: in *Design of Fatigue and Resistant Structures*, ASTM STP 761, 1982, p. 328.
2. W. E. Quist, G. H. Harinarayanan, and A. L. Wingert: in *Aluminum-Lithium Alloys II*, E. A. Starke, Jr. and T. H. Sanders, Jr., eds., TMS-AIME, Warrendale, PA, 1984, p. 313.
3. E. A. Starke, Jr., T. H. Sanders, Jr., and I. G. Palmer: *J. of Metals*, 1981, vol. 33, no. 8, p. 24.
4. W. S. Miller, A. J. Cornish, A. P. Tichener, and D. A. Bennet: in *Aluminum-Lithium Alloys II*, E. A. Starke, Jr. and T. H. Sanders, Jr., eds., TMS-AIME, Warrendale, PA, 1984, p. 355.
5. T. H. Sanders, Jr. and E. A. Starke, Jr., eds., *Aluminum-Lithium Alloys*, TMS-AIME, 1981.
6. E. A. Starke, Jr. and T. H. Sanders, Jr., eds., *Aluminum-Lithium Alloys II*, TMS-AIME, Warrendale, PA, 1984.
7. W. X. Feng, F. S. Lin, and E. A. Starke, Jr.: *Metall. Trans. A*, 1984, vol. 15A, p. 1209.
8. E. A. Starke, Jr. and F. S. Lin: *Metall. Trans. A*, 1982, vol. 13A, p. 2259.
9. B. Noble and G. E. Thompson: *Metal Science Journal*, 1971, vol. 5, p. 114.
10. B. Noble and G. E. Thompson: *Metal Science Journal*, 1972, vol. 6, p. 167.
11. K. Schneider and M. Von Heimendahl: *Z. Metallkde*, 1973, vol. 64 (5), p. 342.
12. F. W. Gayle and J. B. Van der Sande: *Scr. Met.*, 1984, vol. 18, p. 473.
13. P. Hirsch, A. Howie, R. B. Nicholson, D. W. Pashley, and M. J. Whelan: in *Electron Microscopy of Thin Crystals*, R. E. Kreiger Publishing Co., Huntington, NY, 1977, p. 336.
14. C. Laird and H. I. Aaronson: *Trans. TMS-AIME*, 1968, vol. 242, p. 1393.
15. J. M. Silcock: *J. Inst. Met.*, 1959-60, vol. 80, p. 357.
16. B. Noble, I. R. McLauchlin, and G. Thompson: *Acta Metall.*, 1970, vol. 18, p. 339.
17. P. J. Gregson and H. M. Flower: *Acta Metall.*, 1985, vol. 33 (3), p. 532.
18. S. Cersora, G. Cocco, G. Fayherazzi, and L. Schiffini: *Phil. Mag.*, 1977, vol. 35, p. 373.
19. T. H. Sanders and E. A. Starke: *Acta Metall.*, 1982, vol. 36, p. 927.
20. H. Gleiter and E. Hornbogen: *Mat. Sci. Engr.*, 1967/68, vol. 2, p. 285.
21. H. Gleiter and E. Hornbogen: Phys. Stat. Sol., 1965, vol. 12, p. 235.
22. E. Hornbogen and K. H. Zum Gahr: *Metallography*, 1975, vol. 8, p. 181.
23. G. Lütjering and S. Weissman: *Acta Metall.*, 1970, vol. 18, p. 785.
24. E. Hornbogen and G. Lütjering: *6th Intern. Conf. on Light Metals*, Leoben/Vienna, Aluminum Verlag Dusseldorf, 1975, p. 40.
25. A. Gysler, G. Lütjering, and V. Gerold: *Acta Metall.*, 1974, vol. 22, p. 901.
26. G. Terlinde and G. Luetjering: *Metall. Trans. A*, 1982, vol. 13A, p. 1283.
27. P. M. Kelly: *Inter. Met. Rev.*, 1973, vol. 18, p. 31.
28. E. Hornbogen: in *Strength of Metals and Alloys*, R. C. Gifkin, ed., ICSMA 6, 1982, vol. 3, p. 1059.
29. C. J. Beevers: in *Fatigue Thresholds, Fundamentals and Engineering Applications*, J. Backlund, A. F. Blom, and C. J. Beevers, eds., Engineering Materials Advisory Services, Ltd., West Midlands, UK, 1981, vol. 1, p. 257.
30. S. Suresh: Brown University, Providence, RI, private communication, 1985.
31. J. Petit, B. Bouchet, C. Goss, and J. de Fouguet: *Fracture, Proc. 4th Int. Conf. on Fracture (ICF4)*, D. M. R. Taplin, ed., University of Waterloo Press, Waterloo, ON, Canada, 1977, vol. 2, p. 687.
32. A. K. Vasudévan, P. E. Bretz, A. C. Miller, and S. Suresh: *Mater. Sci. and Eng.*, 1984, vol. 64, p. 113.
33. R. D. Carter, E. W. Lee, E. A. Starke, Jr., and C. J. Beevers: *Metall. Trans. A*, 1984, vol. 15A, p. 555.
34. R. L. Donahue, H. M. Clarke, P. Alonanio, R. Kumble, and A. J. McEvily: *Inter. J. of Fract. Mech.*, 1972, vol. 8, p. 209.
35. J. Lindigkeit, G. Terlinde, A. Gysler, and G. Lütjering: *Acta Metall.*, 1979, vol. 27, p. 1717.
36. E. Hornbogen and K-H. Zum Gahr: *Acta Metall.*, 1976, vol. 24, p. 581.
37. S. Suresh: *Metall. Trans. A*, 1985, vol. 16A, p. 249.
38. H. A. Hall: *Corrosion*, June 1967, p. 175.
39. S. Suresh, A. K. Vasudévan, and P. E. Bretz: *Metall. Trans. A*, 1984, vol. 15A, p. 369.
40. S. Suresh and R. O. Ritchie: *Metall. Trans. A*, 1982, vol. 13A, p. 1627.
41. F. S. Lin, S. B. Chakrabortty, and E. A. Starke, Jr.: *Metall. Trans. A*, 1982, vol. 13A, p. 401.
42. A. K. Vasudévan and S. Suresh: *Mater. Sci. and Eng.*, 1985, vol. 72, p. 37.
43. J. M. Silcock, T. J. Heal, and H. K. Hardy: *J. Inst. of Met.*, 1955-56, vol. 84, p. 23.
44. J. D. Boyd and R. B. Nicholson: *Acta Metall.*, 1971, vol. 19, p. 1979.
45. J. T. Staley: *Properties Related to Fracture Toughness*, W. R. Warke, V. Weiss, and G. T. Hahn, eds., ASTM STP 605, ASTM, 1975, p. 71.
46. S. J. Haris, K. Dinsdale, and B. Noble: in *Al-Li Alloys II*, E. A. Starke, Jr. and T. H. Sanders, Jr., eds., TMS-AIME, Warrendale, PA, 1984.
47. G. G. Garret and J. F. Knott: *Metall. Trans. A*, 1978, vol. 9A, p. 1187.
48. G. T. Hahn and A. R. Rosenfield: *Metall. Trans. A*, 1975, vol. 6A, p. 653.
49. J. G. Rinker, M. Marek, and T. H. Sanders, Jr.: in *Aluminum-Lithium Alloys*, E. A. Starke, Jr. and T. H. Sanders, Jr., eds., TMS-AIME, Warrendale, PA, 1984, p. 597.
50. W. W. Gerberich: *Experimental Mechanics*, 1964, vol. 4, p. 335.
51. G. T. Hahn and A. R. Rosenfield: ASTM STP 432, 1968, p. 27.
52. E. Smith, T. S. Cook, and C. A. Rau: *Fracture, Proc. 4th Int. Conf. on Fracture (ICF4)*, D. M. R. Taplin, ed., University of Waterloo Press, Waterloo, ON, Canada, 1977, vol. 1, p. 215.
53. Johaness Weertman: in *Fatigue and Microstructure*, M. Meshii, ed., American Society for Metals, Metals Park, OH, 1979, p. 279.
54. V. Vitek: *J. Mech. Phys. Solids*, 1976, vol. 24, p. 263.
55. J. F. Knott: in *Fundamentals of Fracture Mechanics*, Butterworths & Co. (Publishers) Ltd., London, UK, 1973, p. 89.
56. R. O. Ritchie, W. L. Server, and R. A. Wullaert: *Metall. Trans. A*, 1979, vol. 10A, p. 1557.
57. R. O. Ritchie and A. W. Thompson: *Metall. Trans. A*, 1985, vol. 16A, p. 233.
58. Judith M. Dowling and J. W. Martin: *Acta Metall.*, 1976, vol. 24, p. 1147.
59. J. D. Evensen, N. Ryum, and J. D. Embury: *Mat. Sci. Engr.*, 1975, vol. 18, p. 221.
60. R. F. Ashton, D. S. Thompson, E. A. Starke, Jr., and F. S. Lin: in *Al-Li Alloys III*, C. Baker, P. J. Gregson, S. J. Harris, and C. J. Peel, eds., The Institute of Metals, London, 1986, p. 66.